



**HAL**  
open science

## Degradation of Acetaminophen via UVA-induced advanced oxidation processes (AOPs). Involvement of different radical species: HO $\cdot$ , SO $_4^{\cdot-}$ and HO $_2$ /O $_2^{\cdot-}$

Xiaoning Wang, Marcello Brigante, Wenbo Dong, Zhangxiong Wu, Gilles Mailhot

### ► To cite this version:

Xiaoning Wang, Marcello Brigante, Wenbo Dong, Zhangxiong Wu, Gilles Mailhot. Degradation of Acetaminophen via UVA-induced advanced oxidation processes (AOPs). Involvement of different radical species: HO $\cdot$ , SO $_4^{\cdot-}$  and HO $_2$ /O $_2^{\cdot-}$ . *Chemosphere*, 2020, 258, pp.127268. 10.1016/j.chemosphere.2020.127268 . hal-02995763

**HAL Id: hal-02995763**

**<https://hal.science/hal-02995763>**

Submitted on 9 Nov 2020

**HAL** is a multi-disciplinary open access archive for the deposit and dissemination of scientific research documents, whether they are published or not. The documents may come from teaching and research institutions in France or abroad, or from public or private research centers.

L'archive ouverte pluridisciplinaire **HAL**, est destinée au dépôt et à la diffusion de documents scientifiques de niveau recherche, publiés ou non, émanant des établissements d'enseignement et de recherche français ou étrangers, des laboratoires publics ou privés.

1 **Degradation of Acetaminophen via UVA-induced advanced oxidation**  
2 **processes (AOPs). Involvement of different radical species: HO<sup>•</sup>,**  
3 **SO<sub>4</sub><sup>•-</sup> and HO<sub>2</sub><sup>•</sup>/O<sub>2</sub><sup>•-</sup>**  
4

5 Xiaoning Wang <sup>a, b, c</sup>, Marcello Brigante <sup>b</sup>, Wenbo Dong <sup>c</sup>, Zhangxiong Wu <sup>a</sup>, Gilles  
6 Mailhot <sup>\*b</sup>,

7 **a:** Suzhou Key Laboratory of Green Chemical Engineering, School of Chemical and  
8 Environmental Engineering, College of Chemistry, Chemical Engineering and  
9 Materials Science, Soochow University, Suzhou, Jiangsu 215123, China

10 **b:** Université Clermont Auvergne, CNRS, SIGMA Clermont, Institut de Chimie de  
11 Clermont-Ferrand, F-63000 Clermont-Ferrand, France

12 **c:** Shanghai Key Laboratory of Atmospheric Particle Pollution and Prevention,  
13 Department of Environmental Science and Engineering, Fudan University, Shanghai  
14 200433, China

15 \* Corresponding Author:

16 E-mail: [gilles.mailhot@uca.fr](mailto:gilles.mailhot@uca.fr) (Gilles Mailhot)

17

18

19

20

21

22

1 **Abstract**

2 In this work, UVA radiation that is part of solar light is taken as the irradiation  
3 source and radicals ( $\text{HO}^\bullet$ ,  $\text{SO}_4^{\bullet-}$  and  $\text{HO}_2^\bullet/\text{O}_2^{\bullet-}$ ) are generated through activation of  
4 hydrogen peroxide ( $\text{H}_2\text{O}_2$ ), sodium persulfate ( $\text{Na}_2\text{S}_2\text{O}_8$ ) and Bismuth catalyst  
5 ( $\text{BiOCl}$ ), respectively. The distinguished performance in removing acetaminophen  
6 (ACTP), a model pharmaceutical pollutant, by these three radicals was compared for  
7 the first time. Effect of pH, halide ions concentration and interfacial mechanism have  
8 been investigated in detail. Interestingly, results show that heterogeneous  
9 UVA/ $\text{BiOCl}$  process has higher degradation efficiency than homogeneous  
10 UVA/ $\text{H}_2\text{O}_2$  and UVA/ $\text{Na}_2\text{S}_2\text{O}_8$  systems whatever the solution's pH. To explain these  
11 results, second order reaction rate constant ( $k_{\text{radical,ACTP}}$ ) have been determined with  
12 laser flash photolysis (LFP) or radical scavenging experiments. The strongly  
13 interfacial-dependent  $\text{HO}_2^\bullet/\text{O}_2^{\bullet-}$  radicals have the lowest second order rate constant  
14 with ACTP but highest steady state concentration.  $\text{BiOCl}$  was much easier activated  
15 by UVA, and outstanding ACTP mineralization can be achieved. Combination of  
16  $\text{BiOCl}$  and  $\text{Na}_2\text{S}_2\text{O}_8$  exhibits synergistic effects rather than antagonism effects with  
17  $\text{H}_2\text{O}_2$ . This study highlights the relative effective utilization of solar light through  
18 interfacial directed  $\text{BiOCl}$  photocatalysis and its synergistic effects with traditional  
19 oxidants.

20

21 **Key words:** advanced oxidation process, photocatalysis, UVA, radicals, synergistic  
22 effects

## 1 **1 Introduction**

2 In recent years, advanced oxidation processes (AOPs) have been proposed as  
3 alternative methods to effectively remove persistent organic pollutants (POPs) in  
4 environment. Normally, AOPs have always proved to achieve the best yields in  
5 pollutant destruction when biological treatments are unfeasible, like for endocrine  
6 disrupting chemicals (EDCs) (Pera-Titus et al., 2004; Rosenfeldt and Linden, 2004),  
7 pharmaceuticals or personal care products (PPCPs) (Huber et al., 2003; Abdelmelek et  
8 al., 2011). The predominant oxidation processes are usually based on H<sub>2</sub>O<sub>2</sub> or  
9 persulfate activation by *in situ* production of hydroxyl radical (HO<sup>•</sup>) or sulfate radical  
10 (SO<sub>4</sub><sup>•-</sup>), followed by reaction on the targets pollutants in aqueous solutions  
11 (Andreozzi et al., 1999; Esplugas et al., 2002). Especially, traditional Fenton reaction  
12 (Fe(II)/H<sub>2</sub>O<sub>2</sub>) (Neyens and Baeyens, 2003; Huang et al., 2013) and UV/H<sub>2</sub>O<sub>2</sub> are  
13 predominant strategies to generate HO<sup>•</sup>. Similarly, SO<sub>4</sub><sup>•-</sup> are always produced through  
14 activation of persulfate by heat (Nie et al., 2014), UV, alkalinity (Nie et al., 2019) and  
15 transition metals (Wu et al., 2015a). However, Fenton reactions always suffer from  
16 several limitations like strict acidic solution (pH < 4.0) and iron sludge disposal.

17 At the same time, interfacial based heterogeneous photocatalysis is also one of  
18 the most promising oxidation processes through producing electron (e<sup>-</sup>) and hole (h<sup>+</sup>)  
19 pairs under illumination. HO<sup>•</sup> or hydroperoxyl radicals/superoxide radical anion  
20 (HO<sub>2</sub><sup>•</sup>/O<sub>2</sub><sup>•-</sup>, pKa 4.88) will be subsequently produced by reaction of photogenerated  
21 charge carriers with O<sub>2</sub> and H<sub>2</sub>O (Shaban et al., 2013). Among these photocatalysts,  
22 TiO<sub>2</sub> and its doped products have received a great deal of attention due to its efficient

1 and abundant production of HO<sup>•</sup> (Yang et al., 2008a). Different to TiO<sub>2</sub>, in  
2 bismuth-related photocatalytic process, especially layered BiOX (X = Cl, Br, I)  
3 (Zhang et al., 2008), quenching experiments and theoretical calculation have proved  
4 that they are featured with HO<sub>2</sub><sup>•</sup>/O<sub>2</sub><sup>•-</sup> generation for organic compound degradation  
5 (Tian et al., 2019). Taking BiOCl as catalyst, the photocatalytic process can supply a  
6 simple route to produce HO<sub>2</sub><sup>•</sup>/O<sub>2</sub><sup>•-</sup> effectively. In our last studies, a series of BiOCl  
7 related catalysts have been synthesized by precipitation method successfully followed  
8 with detailed characterization (Wang et al., 2014, 2016a, 2016b). BiOCl possesses  
9 great surface area and suitable valance/conduction band structures to produce  
10 HO<sub>2</sub><sup>•</sup>/O<sub>2</sub><sup>•-</sup> active species, showing excellent performance in removing acetaminophen  
11 (ACTP) from water under irradiation ( $\lambda > 290$  nm), although the band gap value of  
12 BiOCl (~ 3.2 eV) shows that it only can be activated by the ultraviolet light with the  
13 wavelength shorter than 387.5 nm. Similar to the previous literatures, HO<sub>2</sub><sup>•</sup>/O<sub>2</sub><sup>•-</sup>  
14 species are the main radical determined by indirect scavenging experiments.

15 If UVA radiation (315–400 nm) is chosen as the irradiation source, H<sub>2</sub>O<sub>2</sub> and  
16 persulfate as the oxidation sources, the quantum yield comparison between HO<sup>•</sup> and  
17 SO<sub>4</sub><sup>•-</sup> still stay unknown. Furthermore, nobody has compared these two radicals with  
18 HO<sub>2</sub><sup>•</sup>/O<sub>2</sub><sup>•-</sup> under the same experimental conditions. The degradation rate of organic  
19 pollutant depends on the radical concentration, selectivity and oxidizing power. For  
20 these reasons, the distinguished and cumulated effects of these parameters need to be  
21 explored. ACTP was chosen as the model pollutant in this study, because of its heavy  
22 use all over the world. Most of the research on ACTP degradation are mainly based on

1 HO<sup>•</sup> and SO<sub>4</sub><sup>•-</sup> like UV/H<sub>2</sub>O<sub>2</sub> (Andreozzi et al., 2003), Fenton (de Luna et al., 2013),  
2 TiO<sub>2</sub> photocatalyst (Yang et al., 2008b) and persulfate activation (Noorisepehr et al.,  
3 2019; Yun et al., 2019). Its degradation pathway by HO<sup>•</sup> and SO<sub>4</sub><sup>•-</sup> are almost clear,  
4 while its degradation and mineralization abilities by HO<sub>2</sub><sup>•</sup>/O<sub>2</sub><sup>•-</sup> still stays largely  
5 unknown. Furthermore, the combination of TiO<sub>2</sub> with H<sub>2</sub>O<sub>2</sub> (Li et al., 2001) or  
6 persulfate activation (Xu et al., 2019) has been widely investigated. However, rare  
7 studies focus on the synergistic effects between BiOCl with H<sub>2</sub>O or persulfate (Zhang  
8 et al., 2017).

9 In brief, the main goal of this paper is to compare, for the first time, three  
10 different active species HO<sup>•</sup>, SO<sub>4</sub><sup>•-</sup> and HO<sub>2</sub><sup>•</sup>/O<sub>2</sub><sup>•-</sup> produced by UVA/H<sub>2</sub>O<sub>2</sub>,  
11 UVA/Na<sub>2</sub>S<sub>2</sub>O<sub>8</sub> and UVA/BiOCl respectively on the degradation of ACTP. pH and  
12 halide ions (Cl<sup>-</sup> and I<sup>-</sup>) concentration effects on ACTP's degradation have been  
13 investigated in this work. The combination of oxidants in the systems  
14 UVA/BiOCl/H<sub>2</sub>O<sub>2</sub> and UVA/BiOCl/Na<sub>2</sub>S<sub>2</sub>O<sub>8</sub> are also studied to explore the potential  
15 synergistic effects. Interfacial mechanism, mineralization and efficiency of this  
16 process will be explained in detail. Furthermore, second order reaction rate constants  
17 between ACTP and HO<sup>•</sup>, SO<sub>4</sub><sup>•-</sup> or HO<sub>2</sub><sup>•</sup>/O<sub>2</sub><sup>•-</sup> radicals will be determined by laser flash  
18 photolysis (LFP) or competition experiments. The critical affecting parameters on  
19 ACTP's degradation rate will be determined.

## 20 **2 Materials and methods**

### 21 **2.1 Chemicals**

22 BiOCl catalyst was synthesized as in our previous papers (Wang et al., 2016a).

1 ACTP was purchased from Sinopharm Chemical Reagent Co., Ltd. (China).  
2 Bisphenol A (BPA),  $\text{NaH}_2\text{PO}_4 \cdot \text{H}_2\text{O}$ ,  $\text{NH}_4\text{SCN}$ , ethanol (EtOH), tert-butanol (TBA),  
3 sodium persulfate ( $\text{Na}_2\text{S}_2\text{O}_8$ ), benzoquinone (BQ) and potassium iodine (KI) were  
4 obtained from Sigma, France. Hydrogen peroxide ( $\text{H}_2\text{O}_2$ ) solution (30% in water) and  
5 sodium chloride (NaCl) were purchased from Fluka, France.  
6 5,5-Dimethyl-1-pyrroline N-Oxide (DMPO, 98%) was obtained from Adamas  
7 Reagent Co., Ltd. Perchloric acid ( $\text{HClO}_4$ ) and sodium hydroxide (NaOH) were used  
8 to adjust the pH of the solutions. All chemicals were used without further purification,  
9 and milli-Q water was used throughout all the experiments.

## 10 ***2.2 Irradiation setup and experimental procedure***

11 The photocatalytic degradation experiments were performed in a homemade  
12 photoreactor placed in a cylindrical stainless steel container. Four fluorescent  
13 lightbulb lamps (Philips TL D15W/05) were separately placed in the four different  
14 axes while the photoreactor, a water-jacketed Pyrex tube of 2.8 cm internal diameter,  
15 was placed in the center of the setup. The lamp emitting from 300 to 500 nm was used  
16 to simulate UVA solar light; their emission spectrum is shown in **Fig. S1**. 100 mL of  
17 solutions were magnetically stirred with a magnetic bar during irradiation and  
18 experiments were carried out at room temperature ( $293 \pm 2$  K) set by a circulating  
19 cooling water system. Samples were taken from the reaction tube at fixed interval  
20 times and the catalyst solid was removed by  $0.22 \mu\text{m}$  PTFE filters before analysis. In  
21 the experiments, the initial concentrations used were: ACTP  $50 \mu\text{M}$ ,  $\text{H}_2\text{O}_2$  and  
22  $\text{Na}_2\text{S}_2\text{O}_8$  1 mM and  $\text{BiOCl}$  catalyst  $0.3 \text{ g L}^{-1}$  (approximately 1.1 mM). All experiments

1 were performed in duplicates, experimental points represent the averages of two  
2 values, and the error bars indicate the standard deviation.

### 3 ***2.3 Analytical method***

4 The remaining ACTP concentration in the aqueous solution was determined by  
5 high performance liquid chromatography (HPLC) (Alliance, Waters, 2695, USA)  
6 equipped with a photodiode array detector (Waters 2998). A Nucleodur 100-3 C18  
7 reverse column (150 × 2.0 mm, 3.0 μm) was used to separate the compound in the  
8 solution. The flow rate was 0.15 mL min<sup>-1</sup> with a mobile phase mixture of methanol  
9 and water with 0.1% H<sub>3</sub>PO<sub>4</sub> (30/70, v/v). The UV detection of ACTP was set at 244  
10 nm wavelength, and the retention time was 4.9 min. Mineralization of ACTP solution  
11 was followed by total organic carbon (TOC) analysis (5050A, Shimadzu, Japan).  
12 UV-vis spectra were recorded with a Cary 300 UV-visible spectrophotometer. pH  
13 values of the solutions were measured using a Cyberscan 510 pH meter. The zeta  
14 potential of BiOCl was determined by the potentiometric titration method under N<sub>2</sub>  
15 atmosphere at 298 K in 1 mM NaCl solutions. X-ray photoelectron spectroscopy  
16 (XPS) spectra were collected by using a VG Scientific ESCALAB 250Xi  
17 spectrometer (Thermo Fisher Scientific) with C 1s as the calibration standard line.  
18 The optical properties of BiOCl samples were analyzed through the UV-vis diffuse  
19 reflectance (DRS) by Shimadzu UV-3600. The electron spin resonance (ESR)  
20 experiments were carried out on a JES-X320 spectrometer to detect the reactive  
21 radicals generated over the photocatalytic degradation process. As radical probe,  
22 DMPO (100 mM) was used for SO<sub>4</sub><sup>•-</sup>, HO<sup>•</sup> and HO<sub>2</sub><sup>•</sup>/O<sub>2</sub><sup>•-</sup>. ESR spectrum was



1 recorded at room temperature under the following operating conditions: a modulation  
2 frequency of 100 kHz, a sweep width of 0.5 mT, a microwave power of 1 mW, a  
3 microwave frequency of 9.15 GHz and a centerfield of  $326.0 \pm 5$  mT.

#### 4 ***2.4 Determination of the second order rate constant***

5 For the detection of second order rate constant between ACTP and HO<sup>•</sup> ( $k_{\text{ACTP, HO}^{\bullet}}$ ,  
6 HO<sup>•</sup>), LFP method was adopted. Experiments were carried out using the fourth  
7 harmonic ( $\lambda_{\text{exc}} = 266$  nm) of a Quanta Ray GCR 130-01 Nd: YAG laser system  
8 instrument and the energy was set as approximately 45 mJ/pulse. Other conditions  
9 were kept the same to those described in previous articles ([Brigante et al., 2010](#);  
10 [Huang et al., 2018](#)). High concentrated stock solutions (ACTP, H<sub>2</sub>O<sub>2</sub> and SCN<sup>-</sup>) were  
11 mixed just before each experiment and diluted with Mili-Q water to obtain the desired  
12 mixtures and concentrations in a 3 mL quartz cuvette. The value of  $k_{\text{ACTP, HO}^{\bullet}}$  can be  
13 obtained through mixing SCN<sup>-</sup> (0.1 mM), H<sub>2</sub>O<sub>2</sub> (5.5 mM) with different  
14 concentrations of ACTP in the quartz cell. The detection wavelength was set at 475  
15 nm to detect maximum absorbance of SCN<sub>2</sub><sup>•-</sup>. The specific detection calculation was  
16 shown in [Scheme S1](#) and [Equations S1-S4](#).

17 For the detection of second order rate constant of sulfate radical on ACTP ( $k_{\text{ACTP, SO}_4^{\bullet-}}$ ,  
18 SO<sub>4</sub><sup>•-</sup>), competition method was adopted by taking BPA as the competitor ([Ji et al.,](#)  
19 [2013](#)), because  $k_{\text{SO}_4^{\bullet-}, \text{BPA}} = 4.7 \times 10^9 \text{ M}^{-1} \text{ s}^{-1}$  has been detected in previous studies by  
20 LFP ([Huang et al., 2018](#)). For this experiment, BPA (50 μM) and ACTP (50 μM)  
21 were undergoing competition reactions under Na<sub>2</sub>S<sub>2</sub>O<sub>8</sub> (1 mM)/UVA at pH 5.4 for 240  
22 min. At this pH conditions, sulfate radical prevailed with negligible hydroxyl radical

1 existence (Fang et al., 2013a). The concentrations of BPA and ACTP were followed at  
 2 different treatment time intervals and the rate constant of ACTP with  $\text{SO}_4^{\bullet-}$  can be  
 3 calculated through **Eq.1**.

$$4 \quad k_{\text{ACTP},\text{SO}_4^{\bullet-}} = k_{\text{BPA},\text{SO}_4^{\bullet-}} \times \frac{\ln\left(\frac{[\text{ACTP}]_t}{[\text{ACTP}]_0}\right)}{\ln\left(\frac{[\text{BPA}]_t}{[\text{BPA}]_0}\right)} \quad (1)$$

5

### 6 **3 Results and Discussion**

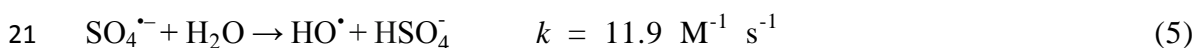
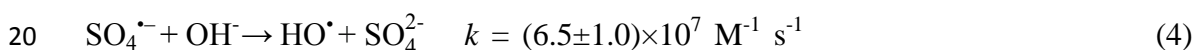
#### 7 **3.1 ACTP degradation in UVA/H<sub>2</sub>O<sub>2</sub> and UVA/Na<sub>2</sub>S<sub>2</sub>O<sub>8</sub> systems under different pH**

8 To explore ACTP's degradation with H<sub>2</sub>O<sub>2</sub> and Na<sub>2</sub>S<sub>2</sub>O<sub>8</sub> under UVA irradiation,  
 9 blank experiments were firstly conducted in the dark to check its stability. ACTP  
 10 alone in aqueous solution is stable between pH 3-9.5 within 40 hours (Fig.S2A). In  
 11 addition, when ACTP was mixed with H<sub>2</sub>O<sub>2</sub> and Na<sub>2</sub>S<sub>2</sub>O<sub>8</sub> (Fig.S2B, C), no detectable  
 12 degradation can be observed until pH 9.0, while at higher pH a degradation was  
 13 measured particularly with persulfate.

14 Degradation of ACTP with H<sub>2</sub>O<sub>2</sub> and Na<sub>2</sub>S<sub>2</sub>O<sub>8</sub> under UVA during irradiation are  
 15 shown in Fig.1, and all the reactions follow pseudo first order reaction kinetics (data  
 16 are shown in Fig.4C). From the control experiment, direct photolysis of ACTP could  
 17 be neglected (Fig.1A). Results of quenching experiments demonstrated that HO<sup>•</sup> and  
 18  $\text{SO}_4^{\bullet-}$  are the predominant radicals involved in the UVA/H<sub>2</sub>O<sub>2</sub> and UVA/Na<sub>2</sub>S<sub>2</sub>O<sub>8</sub>  
 19 system (Eq.2-3) at pH 5.4 respectively by taking IPA (10 mM) and EtOH (1 M) as  
 20 HO<sup>•</sup> ( $k_{\text{IPA}, \text{HO}^{\bullet}} = 1.9 \times 10^9 \text{ M}^{-1} \text{ s}^{-1}$ ) (Wu et al., 2017) and  $\text{SO}_4^{\bullet-}$  ( $k_{\text{EtOH}, \text{SO}_4^{\bullet-}} = 1.6-7.7 \times 10^7$   
 21  $\text{M}^{-1} \text{ s}^{-1}$ ) (Tan et al., 2014) scavengers, respectively. No direct photolysis of ACTP was

1 observed under UVA radiation. With H<sub>2</sub>O<sub>2</sub> or Na<sub>2</sub>S<sub>2</sub>O<sub>8</sub> addition to the solution, ACTP  
 2 shows different degradation kinetics under various pH. In general, UVA/Na<sub>2</sub>S<sub>2</sub>O<sub>8</sub>  
 3 shows a higher degradation efficiency than UVA/H<sub>2</sub>O<sub>2</sub> system whatever the solution's  
 4 pH. It has been reported that H<sub>2</sub>O<sub>2</sub> only can be activated by the light at  $\lambda < 320$  nm,  
 5 which almost have been confirmed in this research for the weak degradation in  
 6 UVA/H<sub>2</sub>O<sub>2</sub> (Li et al., 2001). The obvious degradation of ACTP in UVA/Na<sub>2</sub>S<sub>2</sub>O<sub>8</sub>  
 7 indicates that Na<sub>2</sub>S<sub>2</sub>O<sub>8</sub> is easier to be activated than H<sub>2</sub>O<sub>2</sub> under UVA irradiation.

8 In UVA/H<sub>2</sub>O<sub>2</sub> system, slightly acidic solution has the maximum removal  
 9 percentage rather than acidic and alkaline solutions, although the maximum removal  
 10 is only approximately 10%. In contrast, degradation rate is increasing with pH further  
 11 increasing (Fig.1B) in UVA/Na<sub>2</sub>S<sub>2</sub>O<sub>8</sub> system, and about 57% ACTP can be removed at  
 12 pH 10. At least two reasons are involved simultaneously to account for this  
 13 phenomenon. Firstly, Fig.S2B has been taken into consideration, ACTP is easier to be  
 14 oxidized in anionic form. Furthermore, alkaline solution favors more formation of  
 15 HO<sup>•</sup> radicals from SO<sub>4</sub><sup>•-</sup> than neutral pH (Eq.4-5) (Fang et al., 2013a), and these two  
 16 radicals have different second order reaction rate constants with ACTP, which will be  
 17 explained in the following part.



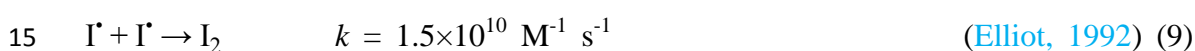
### 22 **3.2 Halide ions (chloride and iodide) effects on ACTP degradation in UVA/H<sub>2</sub>O<sub>2</sub>**

1 *and UVA/Na<sub>2</sub>S<sub>2</sub>O<sub>8</sub> systems*

2 Effects of halide ions were widely studied in previous research works, especially  
3 chloride and bromide (Tamtam and Chiron, 2012; Li et al., 2015). In our study for the  
4 first time the comparison of Cl<sup>-</sup> and I<sup>-</sup>, which is also commonly detected in costal  
5 seawater, saline water or industrial wastewater discharges, were investigated in  
6 UVA/H<sub>2</sub>O<sub>2</sub> and UVA/Na<sub>2</sub>S<sub>2</sub>O<sub>8</sub> systems. In the dark and whatever the systems, the  
7 addition of Cl<sup>-</sup> has no impact on ACTP's concentration change (see Fig.S3). Under  
8 irradiation, the impact of Cl<sup>-</sup> is also very weak. The only effect is observed in the  
9 UVA/H<sub>2</sub>O<sub>2</sub> system, when NaCl is set as 10 mM, the pseudo first order reaction rate  
10 constant increase around 30% (see Fig.S4). In the presence of chloride ions, generated  
11 reactive species such as chlorine radical (Cl<sup>•</sup>) and dichlorine radical anion (Cl<sub>2</sub><sup>•-</sup>)  
12 could react more selectively with electron-rich organic compounds (Grebel et al.,  
13 2010).

14 On the contrary, when iodide ions at same concentrations were added to the  
15 solution, ACTP degradation rates are strongly affected as shown in Fig.2. In the dark,  
16 the addition of KI from 260 μM to 5 mM leads to an increase of the ACTP  
17 degradation with H<sub>2</sub>O<sub>2</sub>, which is much less the case with Na<sub>2</sub>S<sub>2</sub>O<sub>8</sub> at pH 5.4. In the  
18 presence of H<sub>2</sub>O<sub>2</sub> or Na<sub>2</sub>S<sub>2</sub>O<sub>8</sub>, iodide ions could be oxidized to iodine I<sub>2</sub> (Eq.6). Under  
19 UVA irradiation, KI alone in solution has no effect on ACTP (Fig.S5), indicating that  
20 iodide ions under UVA cannot transform or generate any active species. However, in  
21 the presence of H<sub>2</sub>O<sub>2</sub> or Na<sub>2</sub>S<sub>2</sub>O<sub>8</sub> in the KI solution, the photo-degradation rate is  
22 highly enhanced (Fig. 2). In addition, HOI<sup>•-</sup>/I<sup>•-</sup> reactive halogenated species can be

1 generated from HO<sup>•</sup> or SO<sub>4</sub><sup>•-</sup> as shown in **Eq.7-8** (Elliot, 1992), indicating that iodide  
 2 radicals (I<sup>•</sup>, HOI<sup>•-</sup> and I<sub>2</sub><sup>•-</sup>) have higher reactivity with organic pollutants than chloride  
 3 radicals (Yang et al., 2018a). Tamtam and Chiron (2012) and Li et al. (2015) have  
 4 demonstrated that reactive halogenated species reacted more selectively than hydroxyl  
 5 radicals with electron-rich organic pollutants. As ACTP contains hydroxyl and  
 6 acetamido groups, which are electron donors to the aromatic rings, so it is  
 7 hypothesized that these electron-rich moieties may selectively react with these iodide  
 8 related radical reactive species. These selectivity properties of iodide based radicals  
 9 are more emphasized than chloride ions. However, too much higher concentrated  
 10 iodide ions (5 mM) will decrease the efficiency of ACTP degradation by  
 11 self-quenching effects (**Eq.9**).



### 16 **3.3 ACTP's degradation performance in BiOCl/UVA system**

17 Heterogeneous photocatalytic degradation of ACTP has attracted numerous  
 18 attentions recently, and various degradation pathways have been proposed for SO<sub>4</sub><sup>•-</sup>  
 19 and HO<sup>•</sup> reactivity on ACTP. On the contrary, seldom studies have investigated the  
 20 degradation of ACTP predominantly by superoxide radicals. In our previous studies  
 21 (Wang et al., 2016a), BiOCl catalyst has been synthesized following with detailed  
 22 characterization properties, as shown in **Table 1**. The XPS characterization is

1 presented in Fig.S6, the valance state of each element is in accordance with previous  
2 literatures, suggesting that BiOCl is well crystal organized with high purity. With a  
3 relatively wide band-gap (3.2 eV), BiOCl could hardly absorb the light wavelengths  
4 longer than 400 nm (Fig. S7A, B). The valance band of BiOCl determined from XPS  
5 spectra is 2.2 eV (Fig. S7C), which is not positive enough to oxidize H<sub>2</sub>O to form  
6 hydroxyl radicals ( $E^0(\text{H}_2\text{O}/\text{HO}^\bullet) = 2.8 \text{ V vs NHE}$ ) (Wu et al., 2015b). Accordingly, the  
7 conduction band position can be calculated to be -1 eV, that is sufficiently negative  
8 enough to combine with dissolve oxygen to generate  $\text{HO}_2^\bullet/\text{O}_2^{\bullet-}$  ( $E^0(\text{O}_2/\text{O}_2^{\bullet-}) = -0.28 \text{ V}$   
9 vs NHE) (Wu et al., 2015b). Consequently, UVA/BiOCl is adopted to produce  
10  $\text{HO}_2^\bullet/\text{O}_2^{\bullet-}$  radicals, which is further confirmed by quenching experiments (Fig.3A). In  
11 fact, no inhibition is obtained in the presence of TBA (1 mM) and KI (1 mM), which  
12 are traps of hydroxyl radicals and holes. Strong inhibition is noted with BQ (2 mM)  
13 which is able to trap also superoxide radicals. Furthermore, the obvious inhibition in  
14 N<sub>2</sub> purging condition further verifies that  $\text{HO}_2^\bullet/\text{O}_2^{\bullet-}$  originate from the reaction  
15 between dissolved oxygen and electrons.

16 Before irradiation, adsorption capacity of the catalyst is tested and the results  
17 show that less than 10% of ACTP are adsorbed whatever the pH. Under irradiation,  
18 pH effects are investigated and strong increase of the ACTP degradation is observed  
19 at pH 3.0 if we compare with pH 5.8 and 7.5 (Fig.3B). These results are consistent  
20 with previous reports about BiOX used as photocatalyst (Gao et al., 2015; Liang et al.,  
21 2015) and the speciation of  $\text{HO}_2^\bullet/\text{O}_2^{\bullet-}$  (pKa of 4.88) can explain the effect of pH (Li et  
22 al., 2017). Indeed, the second order rate constant between  $\text{O}_2^{\bullet-}$  with phenol is  $5.8 \times 10^2$

1  $\text{M}^{-1} \text{s}^{-1}$  (Tsujiimoto et al., 1993) and Kozmér et al. have demonstrated that in acidic  
2 solutions,  $\text{HO}_2^\bullet$  shows a higher reactivity with phenol  $2.7 \times 10^3 \text{ M}^{-1} \text{ s}^{-1}$  (Kozmér et al.,  
3 2014), which is reasonably similar for phenolic compound ACTP. Furthermore,  
4 Zeta-potential of BiOCl is more negative with pH increasing (see Fig.3C), so less  
5 photo-induced electrons can transferred to the surface to combine with oxygen  
6 because electrostatic repulsion. While, as discussed above, electrons are crucial to  
7 form  $\text{HO}_2^\bullet/\text{O}_2^{\bullet-}$ . In terms of organic compounds mineralization, UVA/BiOCl shows  
8 excellent degradation and mineralization abilities compare to  $\text{H}_2\text{O}_2$  or  $\text{Na}_2\text{S}_2\text{O}_8$   
9 whatever the solution's pH (Fig.3D).

#### 10 ***3.4 Heterogeneous interfacial mechanism in UVA/BiOCl***

11 For heterogeneous photocatalytic degradation, interfacial mechanism is essential  
12 to be investigated to confirm if the reaction is occurring in the solution or on the  
13 surface of catalyst. To clarify this question,  $\text{NaH}_2\text{PO}_4$  has been proved to be a perfect  
14 desorbent in our experiment. Because  $\text{NaH}_2\text{PO}_4$  could occupy almost all the  
15 adsorption sites on the surface of catalyst, and the surface was tightly surrounded by  
16  $\text{NaH}_2\text{PO}_4$  molecules instead of ACTP (Wang et al., 2018). With the addition of  
17  $\text{NaH}_2\text{PO}_4$ , the degradation rate and removal percentage are both strongly suppressed  
18 (Fig.4A). As we discussed above, the main active species  $\text{HO}_2^\bullet/\text{O}_2^{\bullet-}$  comes from the  
19 combination of dissolved oxygen in water and conduction band electrons. With a very  
20 short half-life time,  $\text{HO}_2^\bullet/\text{O}_2^{\bullet-}$  would easily undergo disproportionation (Liang et al.,  
21 2015). Consequently, the fast and direct contact of pollutant and catalyst surface is  
22 crucial for the reaction. Furthermore, BiOCl nanosheets prepared in alkaline

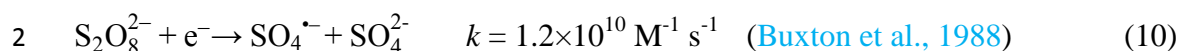
1 conditions in this research were usually dominated with high [010] facets exposure.  
2 The [010] facets possessed open channels and abundant unsaturated Lewis/base sites,  
3 which was helpful for intimate contact between the interfacial surface and organic  
4 molecules (Jiang et al., 2012). So in this photocatalytic degradation system,  
5 degradation reactions must be occurred on the surface or very close to the surface of  
6 the catalyst.

### 7 ***3.5 Combination effects between H<sub>2</sub>O<sub>2</sub>, Na<sub>2</sub>S<sub>2</sub>O<sub>8</sub> and BiOCl under UVA***

8 Degradation of ACTP is investigated in H<sub>2</sub>O<sub>2</sub>/BiOCl/UVA and  
9 Na<sub>2</sub>S<sub>2</sub>O<sub>8</sub>/BiOCl/UVA systems to explore the possible synergy effects between H<sub>2</sub>O<sub>2</sub> or  
10 Na<sub>2</sub>S<sub>2</sub>O<sub>8</sub> and BiOCl, as shown in Fig.4B, C. It is obvious that UVA/BiOCl/Na<sub>2</sub>S<sub>2</sub>O<sub>8</sub> ( $k$  =  
11  $7.13 \times 10^{-4} \text{ s}^{-1}$ ) exhibit strong synergy effects compared with UVA/Na<sub>2</sub>S<sub>2</sub>O<sub>8</sub> ( $k$  =  
12  $4.63 \times 10^{-5} \text{ s}^{-1}$ ) and UVA/BiOCl ( $k = 1.42 \times 10^{-4} \text{ s}^{-1}$ ) through accelerating ACTP's  
13 removal and mineralization rate (Fig.4B, 3D). The increased degradation can be  
14 ascribed to the following reasons. Firstly, the direct photolysis of S<sub>2</sub>O<sub>8</sub><sup>2-</sup> generating  
15 SO<sub>4</sub><sup>•-</sup> could contribute to the oxidation of ACTP. Secondly, S<sub>2</sub>O<sub>8</sub><sup>2-</sup> also can trap the  
16 photogenerated conduction band electrons result in the formation of SO<sub>4</sub><sup>•-</sup> (Eq.10)  
17 (Sarwan et al., 2012). For the third reason, previous research has demonstrated the  
18 reaction of O<sub>2</sub><sup>•-</sup> with persulfate anion to generate SO<sub>4</sub><sup>•-</sup> according to Eq.11 (Fang et  
19 al., 2013b). However, addition of H<sub>2</sub>O<sub>2</sub> slows down the degradation rate associated  
20 with TOC removal (Fig.4B, C and 3D). The higher O–O bond energy of H<sub>2</sub>O<sub>2</sub>  
21 compared with the band in free persulfate ions under natural pH could explain why  
22 persulfate is easier to be activated than H<sub>2</sub>O<sub>2</sub> by the same ROS (reactive oxygen



1 species) (Zhang et al., 2017).



4 ESR spectrum was performed to confirm the active species formed in this system  
5 (Fig.5). No signal was detected in UVA/BiOCl system even repeat for several times or  
6 with higher catalyst loading. This result is consistent with the results in paragraph 3.4,  
7 which indicates that  $\text{HO}_2^{\bullet}/\text{O}_2^{\bullet-}$  species may mainly exist on the surface of catalyst,  
8 leaving trace amount dissolved in aqueous solutions, which is too low to be detected.  
9 With the addition of  $\text{H}_2\text{O}_2$  to the photocatalytic process, very weak  $\text{HO}^{\bullet}$  signals can be  
10 observed due to its trace concentrations. While, with the addition of  $\text{Na}_2\text{S}_2\text{O}_8$ , stronger  
11  $\text{HO}^{\bullet}$  signal associating with  $\text{HO}_2^{\bullet}/\text{O}_2^{\bullet-}$  signal can be observed. It is well known that  
12  $\text{SO}_4^{\bullet-}$ -DMPO is very hard to be detected because of its rapid transformation to  
13  $\text{HO}^{\bullet}$ -DMPO (Yang et al., 2018b).  $\text{SO}_4^{\bullet-}$  is indeed the main active species in natural  
14 and acidic solutions. Above all, the addition of  $\text{Na}_2\text{S}_2\text{O}_8$  facilitates the formation of  
15  $\text{SO}_4^{\bullet-}$  and make full use of  $\text{HO}_2^{\bullet}/\text{O}_2^{\bullet-}$  by driving them from surface to aqueous  
16 solutions, which all contribute to higher mineralization abilities as shown in Fig.3D.

### 17 ***3.6 Determination of second order reaction rate constant between ACTP and $\text{HO}^{\bullet}$ ,*** 18 ***$\text{SO}_4^{\bullet-}$ and $\text{HO}_2^{\bullet}/\text{O}_2^{\bullet-}$ radicals***

19 From the results discussed above, conclusions can be drawn that under same  
20 illuminations, the degradation rate of ACTP follows:  $\text{UVA/BiOCl} > \text{UVA/Na}_2\text{S}_2\text{O}_8 >$   
21  $\text{UVA/H}_2\text{O}_2$ , which mainly depends on the second order reaction rate constant ( $k_{\text{ACTP}}$ ,  
22 radical) and radical's concentrations.  $k_{\text{ACTP,HO}^{\bullet}}$  was determined from Eq.S1-S4 and

1 **Scheme S1**, by following the absorbance of  $\text{SCN}_2^{\bullet-}$  at 475 nm using different ACTP  
2 concentrations. The absorbance decreased from 0.021 to 0.006 when concentration of  
3 ACTP increases from 0 to  $2.33 \times 10^{-4}$  M (**Fig.S8A**), because ACTP compete with  
4  $\text{SCN}^-$  to react with  $\text{HO}^\bullet$ . The slope “a” can be obtained from the linear regression of  
5  $\text{Abs}_0/\text{Abs}$  versus different ACTP concentrations, and it was equal to 11276. Thus the  
6 second order constant  $k_{\text{ACTP},\text{HO}^\bullet}$  can be evaluated from the product of “a”,  
7 concentration of  $\text{SCN}^-$  ( $1 \times 10^{-4}$  M) and  $k_{\text{HO}^\bullet,\text{SCN}^-} = 1.2 \times 10^{10} \text{ M}^{-1} \text{ s}^{-1}$  (**Motohashi and**  
8 **Saito, 1993**), finally it was calculated to be  $1.35 \times 10^{10} \text{ M}^{-1} \text{ s}^{-1}$ .

9 From competition method (**Fig.S8B**),  $k_{\text{SO}_4^{\bullet-},\text{ACTP}} = 6.44 \times 10^9 \text{ M}^{-1} \text{ s}^{-1}$  was  
10 determined. For  $k_{\text{HO}_2^\bullet/\text{O}_2^{\bullet-},\text{ACTP}}$ , reference’s results, already mentioned in part 3.3  
11 ( $5.8 \times 10^2 \text{ M}^{-1} \text{ s}^{-1}$  for  $\text{O}_2^{\bullet-}$  and  $2.7 \times 10^3 \text{ M}^{-1} \text{ s}^{-1}$  for  $\text{HO}_2^\bullet$ ) are took into account and  
12 because it has similar oxidation abilities towards phenolic compounds.

13 The steady state concentration of each radical ( $[\text{Radical}]_{\text{SS}}$ ) can be estimated  
14 from the pseudo first degradation constant of ACTP in three systems determined in  
15 **Fig.S8C**. Considering that the pseudo first-order kinetic constant ( $k'$ ,  $\text{s}^{-1}$ ) is equal to  
16  $k_{\text{radical},\text{ACTP}} \times [\text{Radical}]_{\text{SS}}$ , we can estimate the steady state concentration of each  
17 radical as  $[\text{Radical}]_{\text{SS}} = k_{\text{radical},\text{ACTP}} / k'$ , where  $k_{\text{radical},\text{ACTP}}$  is the second order rate  
18 constant between ACTP and selected radical. Under adopted experimental conditions,  
19 a steady state concentration of  $\text{HO}^\bullet$  and  $\text{SO}_4^{\bullet-}$  was determined to be  $1.0 \times 10^{-15}$  and  
20  $7.2 \times 10^{-15}$  M respectively while for  $\text{HO}_2^\bullet/\text{O}_2^{\bullet-}$  was in the range  $10^{-8}$ - $10^{-7}$  M (**Table 2**).  
21 Although  $\text{HO}_2^\bullet/\text{O}_2^{\bullet-}$  radical has the weakest oxidation capacities, its concentration is  
22 7-8 orders of magnitude higher than  $\text{HO}^\bullet$  and  $\text{SO}_4^{\bullet-}$  radicals, thus directing the fast

1 degradation and mineralization efficiency of ACTP. From the view of economic,  $\text{H}_2\text{O}_2$   
2 and  $\text{Na}_2\text{S}_2\text{O}_8$  are cheaper than the as-prepared BiOCl. But, it's essential to note that,  
3  $\text{H}_2\text{O}_2$  and  $\text{Na}_2\text{S}_2\text{O}_8$  are gradually consumed in solution under irradiation and as a  
4 contrary, BiOCl catalyst, which is stable and can be preserved after catalytic reaction,  
5 has the advantage of easy recovery and so to be recyclable.

## 6 **Conclusion**

7 In summary, heterogeneous photocatalytic process UVA/BiOCl was always more  
8 efficient than the homogeneous UVA/ $\text{H}_2\text{O}_2$  and UVA/ $\text{Na}_2\text{S}_2\text{O}_8$  processes to degrade  
9 ACTP whatever the solution's pH. Halide ions such  $\text{Cl}^-$  plays a negligible role in  
10 UVA/ $\text{H}_2\text{O}_2$  and UVA/ $\text{Na}_2\text{S}_2\text{O}_8$  systems, while  $\text{I}^-$  could significantly improve the  
11 degradation performance due to the reactive species formation. BiOCl catalyst can be  
12 efficiently activated by solar light than traditional oxidant such as  $\text{H}_2\text{O}_2$  and  $\text{Na}_2\text{S}_2\text{O}_8$ .  
13 With the same amount of oxidant or catalyst loading, UVA/BiOCl system could  
14 produce higher concentration of  $\text{HO}_2^\bullet/\text{O}_2^{\bullet-}$  radicals, compared to  $\text{HO}^\bullet$  and  $\text{SO}_4^{\bullet-}$ . This  
15 surface-depended  $\text{HO}_2^\bullet/\text{O}_2^{\bullet-}$  oxidation process could induce significant mineralization  
16 abilities. Addition of  $\text{Na}_2\text{S}_2\text{O}_8$  shows synergistic effects in UVA/BiOCl compared to  
17 the addition of  $\text{H}_2\text{O}_2$ . This research could provide implications in heterogeneous  
18 photocatalyst utilization, and shed light on capable combinations between  
19 photocatalyst and oxidants in future wastewater treatment under solar light irradiation.

## 20 **Acknowledgement**

21 Financial support from the National Natural Science Foundation of China (No.  
22 21875153 and 21906111), the China Postdoctoral Science Foundation

1 (2019M661933), Natural Science Research of Jiangsu Higher Education Institutions  
2 (19KJB610006), and the Young Thousand Talented Program are greatly appreciated.  
3 The authors gratefully acknowledge financial support from China Scholarship  
4 Council for Xiaoning Wang to study at the University Clermont Auvergne, France.  
5 Authors acknowledge financial support from the Region Council of Auvergne, from  
6 the “Fédération des Recherches en Environnement” through the CPER  
7 “Environment” founded by the Region Auvergne, the French government, FEDER  
8 from the European Community from PRC program CNRS/NSFC n°270437 and from  
9 CAP 20-25 I-site project.

10

## 11 **References**

- 12 Abdelmelek, S.B., Greaves, J., Ishida, K.P., Cooper, W.J., Song, W., 2011. Removal of  
13 pharmaceutical and personal care products from reverse osmosis retentate using advanced  
14 oxidation processes. *Environ. Sci. Technol.* 45, 3665-3671.
- 15 Andreozzi, R., Caprio, V., Insola, A., Marotta, R., 1999. Advanced oxidation processes (AOP) for  
16 water purification and recovery. *Catal. Today* 53, 51-59.
- 17 Andreozzi, R., Caprio, V., Marotta, R., Vogna, D., 2003. Paracetamol oxidation from aqueous  
18 solutions by means of ozonation and H<sub>2</sub>O<sub>2</sub>/UV system. *Water Res.* 37, 993-1004.
- 19 Brigante, M., Charbouillot, T., Vione, D., Mailhot, G., 2010. Photochemistry of  
20 1-Nitronaphthalene: a potential source of singlet oxygen and radical species in atmospheric waters.  
21 *J. Phys. Chem. A* 114, 2830-2836.
- 22 Buxton, G.V.; Greenstock, C.L.; Helman, W.P.; Ross, A.B., 1988. Critical review of rate constants  
23 for reactions of hydrated electrons, hydrogen atoms and hydroxyl radicals ( $\cdot\text{OH}/\cdot\text{O}$ ) in aqueous  
24 solution. *J. Phys. Chem. Ref. Data* 17, 513-886
- 25 de Luna, M.D.G., Briones, R.M., Su, C.-C., Lu, M.-C., 2013. Kinetics of acetaminophen  
26 degradation by Fenton oxidation in a fluidized-bed reactor. *Chemosphere* 90, 1444-1448.
- 27 Deng, J., Shao, Y., Gao, N., Xia, S., Tan, C., Zhou, S., Hu, X., 2013. Degradation of the  
28 antiepileptic drug carbamazepine upon different UV-based advanced oxidation processes in water.  
29 *Chem. Eng. J.* 222, 150-158.
- 30 Elliot, A.J., 1992. A pulse radiolysis study of the reaction of OH with I<sub>2</sub> and the decay of I<sub>2</sub><sup>-</sup>. *Can. J.*  
31 *Chem.-Rev. Can. Chim.* 70, 1658-1661.
- 32 Esplugas, S., Gimenez, J., Contreras, S., Pascual, E., Rodríguez, M., 2002. Comparison of  
33 different advanced oxidation processes for phenol degradation. *Water Res.* 36, 1034-1042.

1 Fang, G.-D., Dionysiou, D.D., Zhou, D.-M., Wang, Y., Zhu, X.-D., Fan, J.-X., Cang, L., Wang,  
2 Y.-J., 2013a. Transformation of polychlorinated biphenyls by persulfate at ambient temperature.  
3 *Chemosphere* 90, 1573-1580.

4 Fang, G.-D., Dionysiou, D.D., Al-Abed, S.R., Zhou, D.-M., 2013b. Superoxide radical driving the  
5 activation of persulfate by magnetite nanoparticles: Implications for the degradation of PCBs.  
6 *Appl. Catal. B* 129, 325-332.

7 Gao, X., Zhang, X., Wang, Y., Peng, S., Yue, B., Fan, C., 2015. Photocatalytic degradation of  
8 carbamazepine using hierarchical BiOCl microspheres: Some key operating parameters,  
9 degradation intermediates and reaction pathway. *Chem. Eng. J.* 273, 156-165.

10 Grebel, J.E., Pignatello, J.J., Mitch, W.A., 2010. Effect of halide ions and carbonates on organic  
11 contaminant degradation by hydroxyl radical-based advanced oxidation processes in saline waters.  
12 *Environ. Sci. Technol.* 44, 6822-6828.

13 Huang, W., Brigante, M., Wu, F., Mousty, C., Hanna, K., Mailhot, G., 2013. Assessment of the Fe  
14 (III)-EDDS complex in Fenton-like processes: from the radical formation to the degradation of  
15 bisphenol A. *Environ. Sci. Technol.* 47, 1952-1959.

16 Huang W., Bianco A., Brigante M., Mailhot G., 2018. UVA-UVB activation of hydrogen peroxide  
17 and persulfate for advanced oxidation processes: Efficiency, mechanism and effect of various  
18 water constituents. *J. Hazard. Mater.* 347, 279-287.

19 Huber, M.M., Canonica, S., Park, G.-Y., Von Gunten, U., 2003. Oxidation of pharmaceuticals  
20 during ozonation and advanced oxidation processes. *Environ. Sci. Technol.* 37, 1016-1024.

21 Ji, Y., Zhou, L., Zhang, Y., Ferronato, C., Brigante, M., Mailhot, G., Yang, X., Chovelon, J.M.,  
22 2013. Photochemical degradation of sunscreen agent 2-phenylbenzimidazole-5-sulfonic acid in  
23 different water matrices. *Water Res.* 47, 5865-5875.

24 Jiang, J., Zhao, K., Xiao, X., Zhang, L., 2012. Synthesis and facet-dependent photoreactivity of  
25 BiOCl single-crystalline nanosheets. *J. Am. Chem. Soc.* 134, 4473-4476.

26 Kozmér, Z., Arany, E., Alapi, T., Takács, E., Wojnárovits, L., Dombi, A., 2014. Determination of  
27 the rate constant of hydroperoxyl radical reaction with phenol. *Radiat. Phys. Chem.* 102, 135-138.

28 Li, X., Chen, C., Zhao, J., 2001. Mechanism of Photodecomposition of H<sub>2</sub>O<sub>2</sub> on TiO<sub>2</sub> Surfaces  
29 under Visible Light Irradiation. *Langmuir* 17, 4118-4122.

30 Li, Y., Pan, Y., Lian, L., Yan, S., Song, W., Yang, X., 2017. Photosensitized degradation of  
31 acetaminophen in natural organic matter solutions: The role of triplet states and oxygen. *Water Res.*  
32 109, 266-273.

33 Li, Y., Song, W., Fu, W., Tsang, D.C.W., Yang, X., 2015. The roles of halides in the acetaminophen  
34 degradation by UV/H<sub>2</sub>O<sub>2</sub> treatment: Kinetics, mechanisms, and products analysis. *Chem. Eng. J.*  
35 271, 214-222.

36 Liang, J., Shan, C., Zhang, X., Tong, M., 2015. Bactericidal mechanism of BiOI-AgI under visible  
37 light irradiation. *Chem. Eng. J.* 279, 277-285.

38 Motohashi, N., Saito, Y., 1993. Competitive measurement of rate constants for hydroxyl radical  
39 reactions using radiolytic hydroxylation of benzoate. *Chem. Pharm. Bull.* 41, 1842-1845.

40 Neyens, E., Baeyens, J., 2003. A review of classic Fenton's peroxidation as an advanced oxidation  
41 technique. *J. Hazard. Mater.* 98, 33-50.

42 Nie, M., Yang, Y., Zhang, Z., Yan, C., Wang, X., Li, H., Dong, W., 2014. Degradation of  
43 chloramphenicol by thermally activated persulfate in aqueous solution. *Chem. Eng. J.* 246,  
44 373-382.

1 Nie, M., Zhang, W., Yan, C., Xu, W., Wu, L., Ye, Y., Hu, Y., Dong, W., 2019. Enhanced removal of  
2 organic contaminants in water by the combination of peroxymonosulfate and carbonate. *Sci. Total.*  
3 *Environ.* 647, 734-743.

4 Noorisepehr, M., Ghadirinejad, K., Kakavandi, B., Ramazanpour Esfahani, A., Asadi, A., 2019.  
5 Photo-assisted catalytic degradation of acetaminophen using peroxymonosulfate decomposed by  
6 magnetic carbon heterojunction catalyst. *Chemosphere* 232, 140-151.

7 Pera-Titus, M., Garcia-Molina, V., Baños, M.A., Giménez, J., Esplugas, S., 2004. Degradation of  
8 chlorophenols by means of advanced oxidation processes: a general review. *Appl. Catal. B* 47,  
9 219-256.

10 Rosenfeldt, E.J., Linden, K.G., 2004. Degradation of endocrine disrupting chemicals bisphenol A,  
11 ethinyl estradiol, and estradiol during UV photolysis and advanced oxidation processes. *Environ.*  
12 *Sci. Technol.* 38, 5476-5483.

13 Sarwan, B., Pare, B., Acharya, A.D., Jonnalagadda, S.B., 2012. Mineralization and toxicity  
14 reduction of textile dye neutral red in aqueous phase using BiOCl photocatalysis. *J. Photoch.*  
15 *Photobio. B* 116, 48-55.

16 Shaban, Y.A., El Sayed, M.A., El Maradny, A.A., Al Farawati, R.K., Al Zobidi, M.I., 2013.  
17 Photocatalytic degradation of phenol in natural seawater using visible light active carbon modified  
18 (CM)-n-TiO<sub>2</sub> nanoparticles under UV light and natural sunlight illuminations. *Chemosphere* 91,  
19 307-313.

20 Tamtam, F., Chiron, S., 2012. New insight into photo-bromination processes in saline surface  
21 waters: the case of salicylic acid. *Sci. Total. Environ.* 435-436, 345-350.

22 Tan, C., Gao, N., Zhou, S., Xiao, Y., Zhuang, Z., 2014. Kinetic study of acetaminophen  
23 degradation by UV-based advanced oxidation processes. *Chem. Eng. J.* 253, 229-236.

24 Tian, F., Li, G., Zhao, H., Chen, F., Li, M., Liu, Y., Chen, R., 2019. Residual Fe enhances the  
25 activity of BiOCl hierarchical nanostructure for hydrogen peroxide activation. *J. Catal.* 370,  
26 265-273.

27 Tsujimoto, Y., Hashizume H., Yamazaki M., 1993. Superoxide radical scavenging activity of  
28 phenolic compounds. *Int. J. Biochem.* 25, 491-494.

29 Wang, X., Zhang, Z., Xue, Y., Nie, M., Li, H., Dong, W., 2014. Low crystallized BiOCl<sub>0.75</sub>I<sub>0.25</sub>  
30 synthesized in mixed solvent and its photocatalytic properties under simulated solar irradiation.  
31 *Mater. Lett.* 136, 30-33.

32 Wang, X., Bi, W., Zhai, P., Wang, X., Li, H., Mailhot, G., Dong, W., 2016a. Adsorption and  
33 photocatalytic degradation of pharmaceuticals by BiOCl<sub>x</sub>I<sub>y</sub> nanospheres in aqueous solution. *Appl.*  
34 *Surf. Sci.* 360, 240-251.

35 Wang, X., Chen, H., Li, H., Mailhot, G., Dong, W., 2016b. Preparation and formation mechanism  
36 of BiOCl<sub>0.75</sub>I<sub>0.25</sub> nanospheres by precipitation method in alcohol–water mixed solvents. *J. Colloid*  
37 *Interf. Sci.* 478, 1-10.

38 Wang, X., Brigante, M., Mailhot, G., Dong, W., 2018. Bismuth catalyst mediated degradation of  
39 p-hydroxyphenylacetic acid: Photoactivation, interfacial mechanism, and influence of some  
40 critical parameters. *Chem. Eng. J.* 349, 822-828.

41 Wu, Y., Bianco, A., Brigante, M., Dong, W., de Sainte-Claire, P., Hanna, K., Mailhot, G., 2015a.  
42 Sulfate Radical Photogeneration Using Fe-EDDS: Influence of Critical Parameters and Naturally  
43 Occurring Scavengers. *Environ. Sci. Technol.* 49, 14343-14349.

44 Wu, Y., Prulho, R., Brigante, M., Dong, W., Hanna, K., Mailhot, G., 2017. Activation of persulfate

1 by Fe(III) species: Implications for 4-tert-butylphenol degradation. *J. Hazard. Mater.* 322,  
2 380-386.

3 Wu, W., Changzhong, J., Roy, V.A., 2015b. Recent progress in magnetic iron oxide-semiconductor  
4 composite nanomaterials as promising photocatalysts. *Nanoscale* 7, 38-58.

5 Xu, L., Yang, L., Bai, X., Du, X., Wang, Y., Jin, P., 2019. Persulfate activation towards organic  
6 decomposition and Cr(VI) reduction achieved by a novel CQDs-TiO<sub>2-x</sub>/rGO nanocomposite.  
7 *Chem. Eng. J.* 373, 238-250.

8 Yang L., Yu L.E., Ray M.B., 2008a. Photocatalytic oxidation of paracetamol: dominant reactants,  
9 intermediates, and reaction mechanisms. *Environ. Sci. Technol.* 43, 460-465.

10 Yang L., Liya E.Y., Ray M.B., 2008b. Degradation of paracetamol in aqueous solutions by TiO<sub>2</sub>  
11 photocatalysis. *Water Res.* 42, 3480-3488.

12 Yang, X.-y., Wei, H., Li, K.-b., He, Q., Xie, J.-c., Zhang, J.-t., 2018a. Iodine-enhanced ultrasound  
13 degradation of sulfamethazine in water. *Ultrason. Sonochem.* 42, 759-767.

14 Yang, Y., Banerjee, G., Brudvig, G.W., Kim, J.H., Pignatello, J.J., 2018b. Oxidation of Organic  
15 Compounds in Water by Unactivated Peroxymonosulfate. *Environ. Sci. Technol.* 52, 5911-5919.

16 Yun, W.-C., Lin, K.-Y.A., Tong, W.-C., Lin, Y.-F., Du, Y., 2019. Enhanced degradation of  
17 paracetamol in water using sulfate radical-based advanced oxidation processes catalyzed by  
18 3-dimensional Co<sub>3</sub>O<sub>4</sub> nanoflower. *Chem. Eng. J.* 373, 1329-1337.

19 Zhang, T., Chu, S., Li, J., Wang, L., Chen, R., Shao, Y., Liu, X., Ye, M., 2017. Efficient  
20 Degradation of Aqueous Carbamazepine by Bismuth Oxybromide-Activated Peroxide Oxidation.  
21 *Catalysts* 7.

22 Zhang, X., Ai, Z., Jia, F., Zhang, L., 2008. Generalized one-pot synthesis, characterization, and  
23 photocatalytic activity of hierarchical BiOX (X= Cl, Br, I) nanoplate microspheres. *J. Phys. Chem.*  
24 *C* 112, 747-753.